Mesostructure of photoluminescent porous silicon

F. Ruiz,[a] C. Vázquez-López, J. González-Hernández, and David D. Allred[b]
Centro de Investigación y de Estudios Avanzados del Instituto Politécnico Nacional, Unidad Saltillo, Apdo. Postal 663, 25000 Saltillo, Coahuila, México

G. Romero-Paredes and R. Peña-Sierra
Centro de Investigación y de Estudios Avanzados del Instituto Politécnico Nacional, Departamento de Ingenieria Eléctrica, Apdo. Postal 14-740, 07000, México, México

G. Torres-Delgado
Centro de Investigación y de Estudios Avanzados del Instituto Politécnico Nacional, Departamento de Física, Apdo. Postal 14-740, México, México

(Received 15 November 1993; accepted 7 March 1994)

Scanning electron microscopy, atomic force microscopy, and Raman spectroscopy were used to characterize the microstructure of photoluminescent porous silicon (PS) layers formed by the anodic etching (HF:H_2O:ethanol), at various current densities, of *p*-type (100) silicon wafers possessing resistivity in the range 1–2 Ω cm. Existing models for the origin of luminescence in PS are not supported by our observations. Cross-sectional as well as surface atomic force micrographs show the material to be clumpy rather than columnar; rodlike structures are not observed down to a scale of 40 nm. A three-dimensional model of the mesostructure of porous silicon is discussed. Room-temperature Raman scattering measurements show no evidence for *a*-Si:H or polysilanes and the material reported here is composed of 10 nm roughly spherical Si nanocrytallites rather than 3 nm wires postulated in standard quantum confinement models.

I. INTRODUCTION

Since the discovery of the luminescent properties of porous silicon[1] (PS) considerable work has been performed on this material.[2–16] This has been stimulated by the possibility of fabricating optoelectronic devices based on silicon[17] and, as more recently reported, the potential utilization of this material in chemical sensors[18] as well as curiosity about the mechanisms of luminescence. In spite of this interest and in light of what is known about the structure, there is no general agreement upon a model for the origin of the luminescence.

From the literature, one finds that the morphology and luminescent characteristics of PS can be varied over a surprisingly wide range. In order to exploit this material a necessary condition is to understand the correlation between the luminescence and the micro- and nanostructure. Much of the discussion has been focused on whether quantum confinement is responsible for the luminescent properties of PS.[15] According to such approaches, silicon nanowires with characteristic diameters on the order of 1–5 nm are the site of the luminescence. According to some reports, both transmission electron microscopy[19] (TEM) and Raman scattering[20] results provided some evidence that features with these dimensions are present in efficient, emitting samples. However, no one has yet been able to make a direct correlation between particle size as determined by microscopy and luminescence spectrum. A successful comparison would be a key test of the confinement approach. Alternative explanations which have been offered include the association of the visible luminescence with a SiH_x alloy[6,21] or an amorphous silicon component.[9,22–24] It has also been found that the luminescence efficiency is sensitive to oxidation which occurs readily under illumination in air.[25] Interaction with solvents was also shown to affect the energy and efficiency of luminescence.[18,26]

In this article, we present Raman based data and atomic force micrographs (AFM) of both the cross-sectional and surface morphology of the luminescent porous silicon layers prepared under the conditions described in the next section. These observations may provide a strong check to models which attempt to explain the origin of light in all PS samples where it is observed. We have observed that the three-dimensional (3D) mesoscale structure obtained from cross-sectional and plane views is isotropic and composed of approximately spherical regions that are clumped together in aggregates. The spheroidal regions are on the order of 100 nm, several tens of times larger than the columns which have been proposed to form quantum wires. Although the Raman measurements in our samples suggest the presence of particles with smaller dimensions, the AFM images do not clearly support this observation. This result implies that quantum wires, if they exist, may form a collection of oriented fiber bundles or kinked wires in a coral-like or netlike arrangement forming a mesosize cluster.

In addition, Raman scattering show that neither *a*-Si:H nor polysilane models of photoluminescence (PL) in PS can be supported in the case of these samples. Further, it can be seen that standard quantum confinement models may not be applicable due to the Si nanocrystallite size and shape (10 nm diameter, roughly spherical regions). A modification of the standard model which incorporates an additional confinement mechanism of one or more of the carriers may be a profitable direction for future theoretical work.

---
[a]On leave from Instituto de Física de la Universidad Autónoma de San Luis Potosí, México.

[b]On leave from Department of Physics and Astronomy, Brigham Young University, Provo, UT 84602.

 0734-2101/94/12(4)/2565/7/$1.00 ©1994 American Vacuum Society

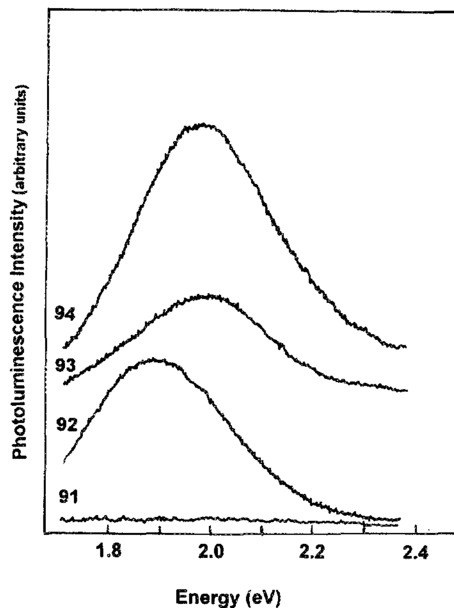

FIG. 1. Room temperature photoluminescence from samples 91, 92, 93, and 94. The emission is observed in the red part of the spectrum and shifts toward higher energies with increasing anodization current.

II. EXPERIMENTAL PROCEDURES

The porous silicon layers used in this work were prepared by anodization in a solution prepared in the standard fashion, that is, concentrated hydrofluoric acid (HF), water, and ethyl alcohol are mixed in the ratio by a volume of 1:1:2. *p*-Type (100) silicon wafers with a resistivity of 1–2 Ω cm were subjected to electrochemical etching in the solution at current densities of 1, 5, 25, and 40 mA/cm^2. Samples prepared with these current densities are referred to as 91, 92, 93, and 94, respectively. In all cases the anodization time was kept constant at 15 min. The negative electrode was a platinum foil. The atomic force images were obtained in air using a commercially available instrument.[27] The images were created using an *xyz* piezotranslator to raster scan the surface laterally at a frequency of 4 Hz. The surface height profiles were recorded in a constant-deflection mode, i.e., feedback electronics were used to keep the deflection and hence the force constant at 1 nN. The room temperature Raman and PL spectra were obtained using for excitation an Ar ion laser tuned to 488 nm. Both measurements were taken from the same region of the sample. Raman and PL measurements were carried out with laser powers of approximately 50 and 10 mW, respectively.

III. RESULTS AND DISCUSSION

Figure 1 shows the PL spectra from samples 91, 92, 93, and 94. Samples 91 did not show a significant PL emission under similar measuring conditions. In agreement with what has been reported, we observed a strong visible emission in the red part of the spectrum. There is also a shift toward higher energies in the position of the emission band with an increase in the anodization current. Using samples prepared by other groups as a reference we observed that the intensity of the emission is comparable to what is observed in efficient samples.

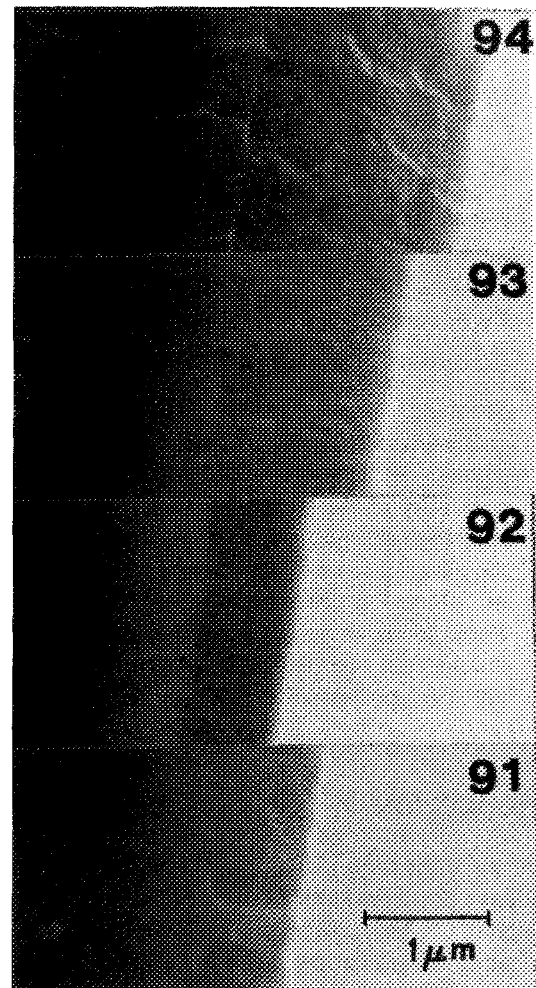

FIG. 2. Typical scanning electron cross-section micrographs of samples 91, 92, 93, and 94 obtained from cleaved samples.

Figure 2 shows typical scanning electron cross-sectional micrographs of samples 91, 92, 93, and 94 obtained from cleaved samples. Sample 91 is characterized by the formation of macropores which develop perpendicular to the etched surface. They possess lateral dimensions as large as one third of a micrometer. For the small anodization current of 1 mA/cm^2, however, the formation of a well-defined porous layer is not evident in the cross-sectional micrographs. A characteristic feature of samples 92, 93, and 94, on the other hand, is the presence of a well-defined interface which delineates the boundaries of the anodization front. From these micrographs one can estimate that the thickness of the porous layer is of about 0.5, 1.3, and 1.8 μm for samples 92, 93, and 94, respectively. We note that there are striking qualitative differences in the microstructure of porous silicon prepared by other groups by apparently similar procedures. TEM cross-sectional images of others[28] show in some cases a columnar structure where column diameters are on the or-

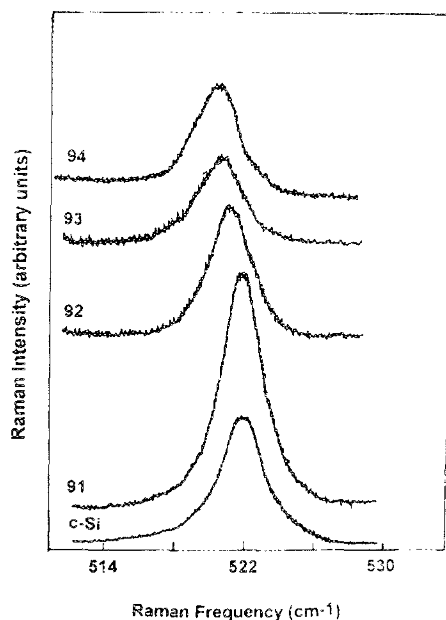

FIG. 3. Raman spectra of samples 91, 92, 93, and 94. For comparison the spectrum of an unetched silicon wafer (bottom) is also shown.

der of 1 μm, and in others an open coral-like microstructure. The scanning electron microscope (SEM) micrographs from our samples provide evidence of a mesostructure similar to those previously reported, that is, a highly porous structure, although the directional etching is not as evident.

Figure 3 shows the Raman data for the 91, 92, 93, and 94 porous silicon samples. For comparison, the spectrum of an unetched silicon wafer (bottom) is also shown. From these data, one sees that there is a gradual downward shift in the peak position and an increasing asymmetric broadening in the Raman line with increasing anodization current density. The shape and position of the Raman line of sample 91 are basically indistinguishable from those of the unetched samples. The peak position for samples 92, 93, and 94 are 521.3, 520.7, and 520.4 cm^{-1}, with an asymmetry of 1, 1, and 1.2, respectively. The asymmetry factor is defined as the ratio of the low- to the high-frequency half-widths of the Raman line; therefore an asymmetry factor of 1 corresponds to a totally symmetric line. The position and width of the symmetric Raman line of the reference sample are of 522 and 3.4 cm^{-1}, respectively. Several authors[29-32] have reported that disorder or finite size effects, which destroy the full translational symmetry of the material, result in changes in the Raman line similar to these we observed. A model has thus been developed and used to estimate the average grain size in nanocrystalline materials and, in particular, in silicon.[29] The model allows for the estimation of the average particle size from either the peak position, peak width, or line asymmetry. In our samples, the average particle size determined using Raman data were >10, ~ 11, and ~ 9 nm for samples 92, 93, and 94, respectively. This estimation is independent of the Raman parameter used for its determination. An agreement between the methods suggests the grains are roughly spherical. Therefore, in agreement with others,[31,32] our results do not support a model of rodlike silicon crystallites, although nanocrystalline grains attached together to form chains or open 3D networks in a low-density structure are not only possible but likely.

The differences between what we observe and what others have seen is also noteworthy. Our peaks are much narrower and less shifted from the position of single crystal silicon than seen in others studies of PS,[20,32] indicative of larger nanocrystallites, as indeed our numerical results confirm. Other groups in using Raman spectroscopy to determine the average size of the nanostructures in porous silicon samples, in general, have found values that are usually in the range of 2–4 nm,[20,32] which is considerably below 10 nm seen in this study. In addition, in some cases contributions from an amorphous component have also been observed[14] for which we see absolutely no evidence. There seems to be no way to interpret the Raman results to make them compatible with others. We note that the changes observed in the Raman line could be associated with structural defects or perturbations in the lattice other than grain boundaries,[30] but these would dictate that the size of the particles would be greater rather than less than 10 nm.

There are other studies which show that 10 nm structures may be dominant or at least play an important role in the nanostructure of some PS samples. STM results of Ref. 33 shows that the average spacing of columns in cleaved luminescent PS may be about 10 nm, in agreement with our Raman measurement of crystallite sizes. It should also be noted that the diameter of the skeletal silicon framework, the dominant structural element, in the coral-like highly porous silicon of Ref. 28 (Fig. 4) is about 10 nm. The fact that particle sizes seen in this and other studies are considerably larger than those invoked in traditional quantum confinement models and that no evidence of amorphous silicon is seen in the samples of this study via Raman scattering may provide a significant check on models that seek to explain the high photoluminescence efficiency of PS in all the types of samples where it is observed.

Figures 4 and 5 are AFM surface images of the four samples displayed at two different scales. In each, the letters (a)–(d) correspond, respectively, to sample numbers 91–94. The micrographs in Figs. 4 and 5 correspond, respectively, to a full width of the scan area of 2.0 and 0.5 μm. The fractal-like nature of the surface morphology is clear, in agreement to similar observations reported in Ref. 22. The maximum vertical scale required to display the full peak to valley height differences decreases with decreasing scan area, being 200 and 40 nm in Figs. 4 and 5, respectively. The surface has a clumpy look at each scale range as if composed of a spherical particle of various diameters. It should be noted that the vertical scale is exaggerated with respect to the horizontal in these figures.

Figure 6 shows a typical AFM cross section of samples 92, 93, and 94 obtained from cleaved material. In the lower part of each of the micrographs the surface is quite smooth. This is the unattacked portion of the silicon wafer. Above it lies the area that was attacked significantly. The boundary between the attacked and unattacked material is jagged but relatively sharp. In the porous silicon region the morphology

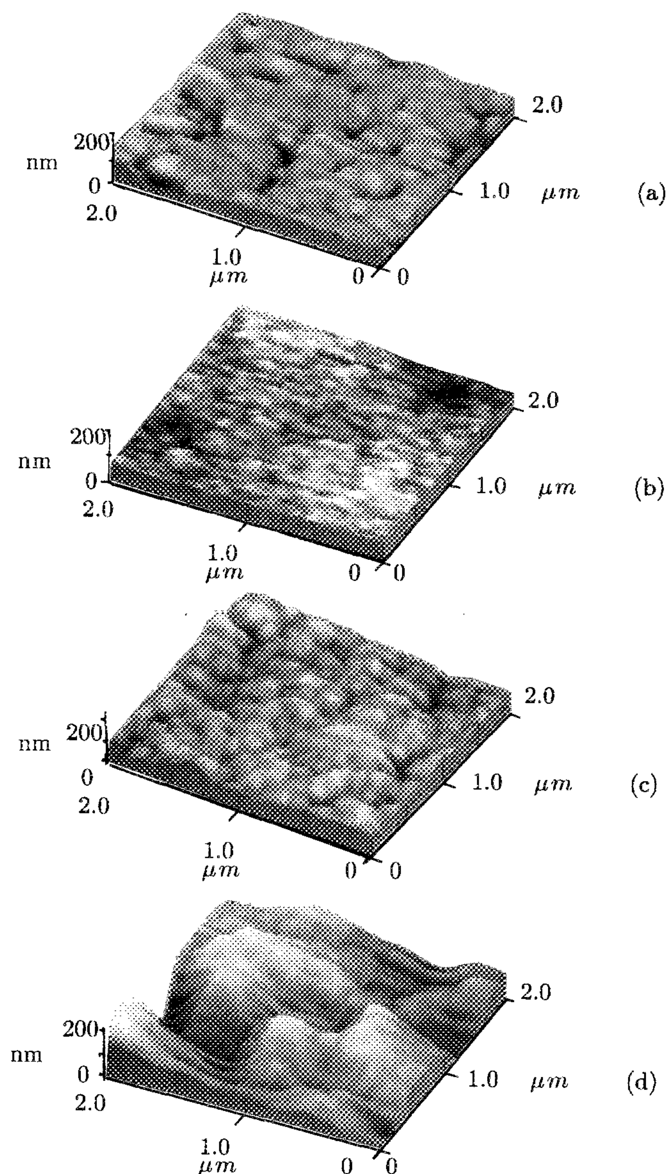

FIG. 4. AFM images of samples 91–94 [(a)–(d)] displayed for a full scan area of 2 μm×2 μm. The vertical scale is 100 nm per division.

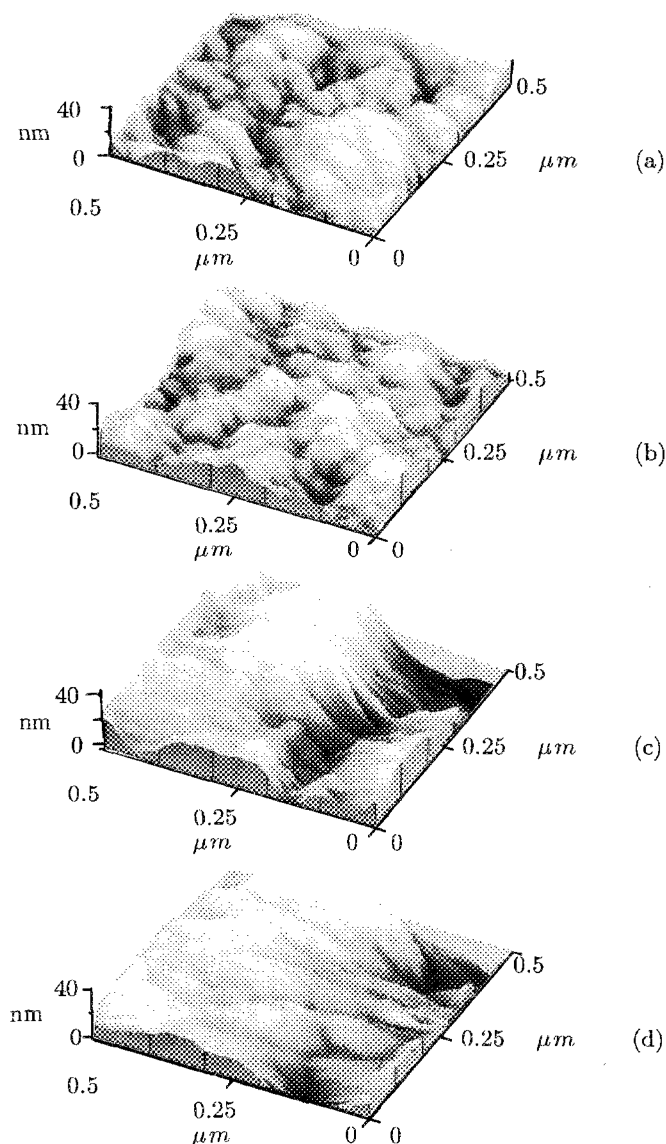

FIG. 5. AFM images of samples 91–94 [(a)–(d)] displayed for a full scan area of 0.5 μm×0.5 μm. The vertical scale is 20 nm per division.

of mountains and hills separated in some parts by valleys is seen. It possesses a morphology very much like the top surface of the PS. Note that the dimensions of the peaks and valleys achieved within a short distance of the interface with the substrate are more or less constant, that is, the structure can be seen to be similar, from near the porous silicon/silicon interface to near the top surface of the PS. We have quantified this observation by making several line profile scans (Fig. 7) parallel to the interface between the attacked and unattacked regions. The line profile scans were taken at equally spaced intervals separated by approximately 300 nm. It is found that within 300 nm of the interface the peak to valley roughness has risen to a value that remains essentially constant throughout the whole thickness of the film, and that the power spectra are essentially the same for all scans.

Plane view images from scans of 100×100 nm^2 from our PS layers show some evidence of what appears to be features with dimensions of less than 100 nm, in some cases as small as 20 nm, however, these are only found in certain areas of the PS layer and therefore are not considered representative of the sample surface. In accordance with the fractal-like behavior observed at larger scales and in agreement with the Raman measurements, surface morphological features of dimensions smaller than those revealed by images in Figs. 4 and 5 are expected. It is also possible that the small particles detected by Raman measurements are clustered together in such a way to form a surface morphology which cannot be reasonably detected by AFM. Atomic size features on very smooth surfaces are detectible, but features smaller than 20 nm are difficult to resolve on surfaces of pronounced roughness and large aspect ratios due to the dimensions of the AFM tip.

Evidence in Fig. 6 of anisotropy or preferential etching in

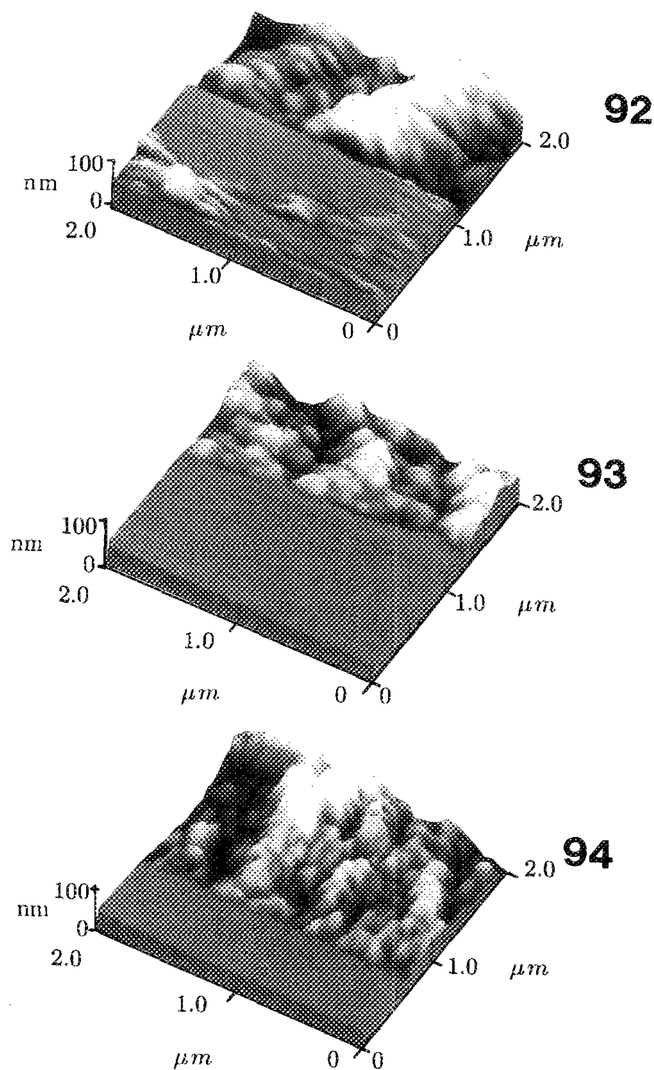

FIG. 6. Typical AFM cross-section view of samples 92, 93, and 94 obtained from cleaved samples.

a direction perpendicular to the surface is not immediately apparent. Close examination shows, however, some evidence of anisotropy. Many of the ridges and valleys seem to be linked and run generally vertically from the top of the film to the unattacked interface. Clearly, they are neither uniform columns nor pores running straight from the surface into the substrate, as are often depicted in schematic diagrams, nor does their morphology resemble the micron-sized pits sometimes observed in SEM micrographs that burrow straight into the wafer. Their route, rather, is twisting and tortuous and their width nonuniform.

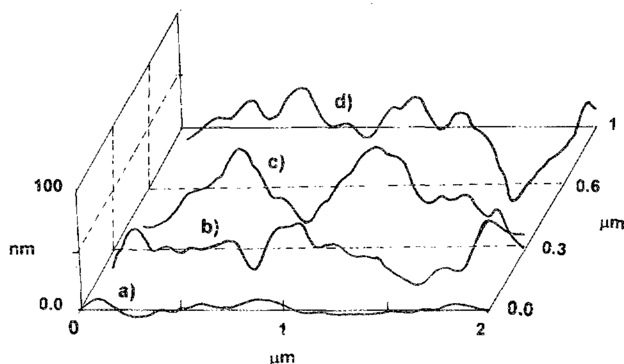

FIG. 7. Line profile scans parallel to the interface between the attacked and nonattacked regions.

It should be noted that the valleys are often wider at the top surface of the film while the hills are generally of a more constant size, which may indicate that the pores are larger at the top and narrow as they go into the substrate as might be expected.

Deductions based on observed morphology of cross sections require, in general, careful interpretation, however. We have good reason to conclude that the sample will cleave along weak spots that would be from pore to pore.[33] One does not know, however, how the face of the sample on the other side of the break appears. In at least some cases the valleys may be matched by mountains and not valleys on the other side, that is, the valley may correspond to a "pull out" rather than a pore. Arguments about a larger pore size near the surface must be tempered by this realization.

An example of this exists. Note that in the upper left corner of Fig. 6, sample 94, there is large valley that may be a void since there is narrow ridge above it. This valley may be due to the penetration of the sample by pores, but it may as well be a pull out where material was removed in the cleaving process. It may be impossible to tell which for any given feature. If, however, as is observed in these images, there are in general more wide valleys near the surface while the dimensions of the mountains remains about the same, then it can be concluded that the pores are generally wider at the top of the porous silicon layer than at the base.

The most noteworthy observation about Fig. 6, however, is that the morphology of the porous region in cross section is very similar to the morphology of the top surfaces of the samples. This suggests that the film mesoscale structure, that is, the structure which corresponds to features possessing characteristic dimensions of several tens of nanometers or larger, is remarkably isotropic and is composed of approximately spherical regions that are aggregated together.

In Fig. 8 we show a picture depicting the 3D mesostructure of porous silicon sample 93 which we derived by combining atomic force micrographs of the cross-sectional and surface morphology. The bottom, that is, the smooth part of the cube, corresponds to the unattacked silicon wafer. Both scales in and perpendicular (not shown) to the main plane are identical. The scales indicating the dimensions of the features in both the plane and cross-sectional views are in nanometers, but are displayed here only for the surface image for clarity. To our knowledge, a 3D image like this has not been previously constructed and may have utility in evaluating some of the current models of porous silicon. It should be noted, for example, that there is no evidence of fibrous structures or isolated wires running from near the unetched region to near the sample surface. The samples have generally a more random appearance, though, as mentioned above, the clumps and pores show some evidence of forming chains that run more or less from bottom to top. The clusters are on

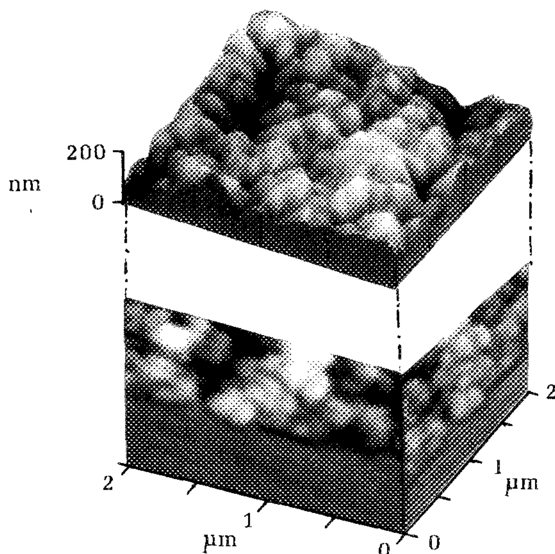

FIG. 8. Picture depicting the three-dimensional mesostructure of porous silicon (sample 93), prepared from cross-sectional and surface AF micrographs.

the order of 100 nm in diameter and thus are many tens of times larger than the columns which have been proposed to form quantum wires. The formation of the clusters appears to be linked to the penetration of large mesopores which percolate through the film, not always perpendicular to the surface of the film. The presence of the clusters has important ramifications for our understanding of the nanostructure of porous silicon and our understanding of the origin of luminescence in PS. It implies that quantum wires, if they exist, may be longer than they are wide but cannot continue the thickness of the film in these samples; rather their average length may be no more than a few hundred nanometers, interrupted by pores. If the prevalence of linked spherical forms which dominates in the mesostructures continues to nanoscales, then the nanostructure of the PS studied here could be expect be resemble the coral-like, 3D open network or what might be termed random wire network observed some cases by TEM.[28] Fractal models were mentioned early in the consideration of PL quality porous silicon.[1] It may be time to give them renewed emphasis.

IV. CONCLUSIONS

We have probed the three-dimensional mesoscale (down to about 25 nm) of photoluminescent porous silicon using atomic force microscopy and present composite images that give a sense that the three-dimensional mesostructure of the material down to a feature size of about 100 nm is dominated by fractal-like, aggregated spherical regions rather than oriented fibrous (quantum wires) structures. Below the range of the AFM we have used Raman spectroscopy to probe for the presence of amorphous regions and polysilane and to measure the average size and shape of Si nanocrystallites. We find that efficient PL is possible in samples where there is no Raman evidence of either a-Si nor SiH_x and where the dominant form of Si is 10 nm diameter, approximately spherical nanocrystallites instead of the much thinner wires required by some spatial quantum confinement models. These observations can be expected to be very useful in evaluating current and forming new models of porous silicon. In particular, we suggested that fractal (random wire) models of the nanostructure of some kinds of PS be more appropriated and that it may be useful to consider mechanisms such as strain or chemical or electrical potentials which might confine the carriers in a small region of the nanocrystallites.

ACKNOWLEDGMENTS

This research was partially supported by Consejo Nacional de Ciencia y Tecnología (CONACYT), México. D.D.A. thanks CONACYT for partial support during the completion of this work and acknowledges with graditude the hospitality of CINVESTAV-IPN, UNIDAD Saltillo.

[1]L. T. Canham, Appl. Phys. Lett. **57**, 1046 (1990).
[2]For a general review up until 1991, see *Light Emission from Silicon*, edited by S. S. Iyer, R. T. Collins, and L. T. Canham [Mater. Res. Soc. Symp. Proc. **256** (1992)].
[3]N. Ookubo, H. Ono, Y. Ochiai, Y. Mochizuki, and S. Matsui, Appl. Phys. Lett. **61**, 940 (1992).
[4]V. Petrova-Koch, T. Muschik, A. Kux, B. K. Meyer, F. Koch, and V. Lehmann, Appl. Phys. Lett. **61**, 943 (1992).
[5]M. Voos, P. H. Uzan, C. Delalande, G. Bastard, and A. Halimaoui, Appl. Phys. Lett. **61**, 1213 (1992).
[6]M. B. Robinson, A. C. Dillon, D. R. Haynes, and S. M. George, Appl. Phys. Lett. **61**, 1414 (1992).
[7]Weimin Zhou, H. Shen, J. F. Harvey, R. A. Lux, M. Dutta, F. Lu, C. H. Perry, R. Tsu, N. M. Kalkhoran, and F. Namavar, Appl. Phys Lett. **61**, 1435 (1992).
[8]S. M. Prokes, W. E. Carlos, and V. M. Bermudez, Appl. Phys. Lett. **61**, 1447 (1992).
[9]J. M. Perez, J. Villalobos, P. McNeill, J. Prasad, R. Cheek, J. Kelber, J. P. Estrera, P. D. Stevens, and R. Glosser, Appl. Phys. Lett. **61**, 563 (1992).
[10]A. V. Andrianov, D. I. Kovalev, V. B. Shuman, and I. D. Yaroshetskii, Semiconductors **27**, 71 (1993).
[11]V. P. Parkhutik, J. M. Albella, J. M. Martínez-Duart, J. M. Gómez-Rodríguez, A. M. Baró, and V. I. Shershulsky, Appl. Phys. Lett. **62**, 366 (1993).
[12]N. Noguchi and I. Suemune, Appl. Phys. Lett. **62**, 1429 (1993).
[13]K. L. Narasimhan, S. Banerjee, A. K. Sirvastava, and A. Sardesai, Appl. Phys. Lett. **62**, 331 (1993).
[14]Y. H. Seo, H.-J. Lee, H. I. Jeon, D. H. Oh, K. S. Nahm, Y. H. Lee, E.-K. Suh, H. J. Lee, and Y. G. Kwang, Appl. Phys. Lett. **62**, 1812 (1993).
[15]M. Koós, I. Pócsik, and E. B. Vázsonyi, Appl. Phys. Lett. **62**, 1797 (1993).
[16]S. Shih, K. H. Jung, D. L. Kwong, M. Kovar, and J. M. White, Appl. Phys. Lett. **62**, 1780 (1993).
[17]L. Canham, Mater. Res. Soc. Bull. July, 22 (1993).
[18]K. H. Li, C. Tsai, J. Srarthy, and J. C. Campbell, Appl. Phys. Lett. **62**, 3192 (1993).
[19]In Ref. 2, p. 7.
[20]R. Tsu, H. Shen, and M. Dutta, Appl. Phys. Lett. **60**, 112 (1992).
[21]C. Tsai, K.-H. Li, J. Sarathy, S. Shih, J. C. Campbell, B. K. Hance, and J. M. White, Appl. Phys. Lett. **58**, 2814 (1991).
[22]T. George, M. S. Anderson, W. T. Pike, T. L. Lin, R. W. Fathauer, K. H. Jung, and D. L. Kwong, Appl. Phys. Lett. **60**, 2359 (1992).
[23]R. W. Fathauer, T. George, A. Ksendzov, T. L. Lin, W. T. Pike, and R. P. Vásquez, Appl. Phys. Lett. **60**, 995 (1992).
[24]R. P. Vásquez, R. W. Fathauer, T. George, A. Ksendzov, and T. L. Lin, Appl. Phys. Lett. **60**, 1004 (1992).
[25]M. A. Tischler, R. T. Collins, J. H. Stathis, and J. C. Tsang, Appl. Phys. Lett. **60**, 639 (1992).
[26]J. L. Coffer, Sean C. Lilley, R. A. Martin, and L. A. Files-Sesler, J. Appl. Phys. **74**, 2094 (1993).
[27]Park Scientific Instruments SFM Model No. SFM-BD2-210.
[28]A. G. Cullis, L. T. Canham, and O. D. Dosser, in Ref. 2, p. 7.
[29]H. Richter, Z. P. Wang, and L. Ley, Solid State Commun. **39**, 625 (1981).

[30]J. González-Hernández, G. H. Azarbayejani, R. Tsu, and F. H. Pollak, Appl. Phys. Lett. **47**, 1350 (1985).
[31]R. Tsu, S. S. Chao, M. Izu, S. R. Ovshinsky, G. J. Jan, and F. H. Pollak, J. Phys. (Paris) Colloq. **42**, C4 269 (1981).
[32]Z. Sui, P. P. Leong, I. P. Herman, G. S. Higashi, and H. Temkin, in Ref. 2, p. 13.
[33]A. Karavansky, M. A. Kachalov, A. P. Maslov, Yu. N. Petrov, V. N. Seleznev, and A. O. Shuvalov, JETP Lett. **57**, 239 (1993).